

Prediction of solid circulation rate in an internal circulating fluidized bed: An empirical and ANN approach

Mona Mary Varghese ^a, Teja Reddy Vakamalla ^{a,*}, Ravi Gujjula ^b, Narasimha Mangadoddy ^c

^a Department of Chemical Engineering, National Institute of Technology Calicut, Kozhikode, Kerala, 673601, India

^b Andhra Pradesh State Skills Development Corporation, Vijayawada, Andhra Pradesh, 522501, India

^c Department of Chemical Engineering, Indian Institute of Technology Hyderabad, Sangareddy, Telangana, 502284, India



ARTICLE INFO

Keywords:

Empirical model
Internal circulating fluidized bed
Hydrodynamics
Solid circulation rate
ANN

ABSTRACT

Internal Circulating Fluidized beds (ICFBs) are interested in various industries because of their higher thermal efficiency and high reaction rates. However, understanding the complex flow hydrodynamics inside an ICFB is challenging. Also, the experiments needed are expensive and time-consuming. Therefore this study aims to predict the solids circulation rate in an in-house ICFB (0.3 m internal diameter x 3.0 m height) using an empirical model and an Artificial Neural Network (ANN) technique. The solid circulation rates measured at different operating and design conditions using a high-speed video camera are utilized to develop the models mentioned earlier. A dimensionless approach and nonlinear regression models are adopted to derive the empirical model. The Analysis of Variance (ANOVA) technique calculates F-number and their corresponding probabilities (P-values). The ANN model is developed with four input variables: particle size, static bed height, gap height, and gas superficial velocity. Multi-layer Perception model (MLP) with the Feedforward Back Propagation learning rule is employed to build the ANN model. A single hidden layer with nine neurons predicted a close solid circulation rate with minimal error over the empirical model compared to experimental data. Further, the empirical and ANN model's predicting capability is tested against literature data.

1. Introduction

Conventional Circulating Fluidized Beds (CFBs) are widely used in industrial reactors, mainly in coal combustion, gasification, and petroleum refineries [1–3]. However, it requires a very tall vessel, such as a solid riser and a cyclone, to externally recycle the separated solids from the gas stream [2,4]. Therefore, Internal Circulating Fluidized Beds (ICFBs) were developed in the 1980s to alleviate the typical operation of CFBs. ICFBs help to promote solid circulation inside a single vessel either by using a centrally placed draft tube or a plate that splits the bed into different sections [4]. The draft tube acts as a fluidized bed riser, and the air input through the annular section helps avoid accumulation at the bottom of the ICFB column and provides smooth solid circulation inside the vessel. The particles are carried upward inside the draft tube while flowing downward in the annular section of an ICFB [5].

Moreover, ICFBs have advantages over conventional CFBs apart from their compact size. The heat loss from the reactor in ICFBs is less than CFBs because the heat from the riser is entirely absorbed by the annular section, which acts as a heat sink. On the other hand, the internal

circulation of particles provides a longer residence time and contact area and results in higher conversion than conventional CFBs [6]. With greater mixing capacity and simple construction, these ICFBs are utilized in coal combustion, coal gasification, desulfurization, solid waste disposal, and continuous absorption and desorption process [7–10].

Understanding the complex gas-solid interactions is challenging in an ICFB, mainly due to the turbulent flow and the vigorous contact between the phases [11]. The continuous circulation of solid particles inside the ICFB demands a complete understanding of the solid circulation behavior. The main factors affecting solid circulation rates are particle size and density, orifice diameter, and the superficial gas velocities of the draft tube and the annulus [6]. In addition, the solid circulation rate is a crucial parameter that determines the performance of the ICFB, as it influences the gas-solid contact efficiency, rate of heat, and mass transfer. It also affects the residence time of solid particles. Thus the knowledge of this hydrodynamic property is essential for designing the ICFB with a draft tube.

Several experimental studies can be found in the literature that focuses on the hydrodynamics of gas-solid flow in an ICFB. Choi and Kim [12] determined the bubble properties and the solid circulation rate in

* Corresponding author.

E-mail address: teja@nitc.ac.in (T.R. Vakamalla).

Nomenclature	
A_d	Draft tube area (m^2)
A_a	Annulus area (m^2)
A_{Gap}	Gap area for the gas to flow (m^2)
d_p	Particle diameter (m)
G_s	Solid circulation rate ($\text{kg}/\text{m}^2\text{s}$)
Re_p	Particle Reynolds number (-)
u_a	Superficial velocity in the annulus (m/s)
u_o	Gas superficial velocity in the draft tube (m/s)
u_{pAN}, u_{pr}	Particle velocity in the annulus and riser (m/s)
<i>Greek Symbols</i>	
ρ_g	Air density (kg/m^3)
ρ_s	Solid density (kg/m^3)
ε_s	Solid volume fraction (-)
μ	Fluid viscosity (kg/ms)
<i>Subscripts</i>	
g	Gas phase
s	Solid phase
<i>Abbreviations</i>	
ANN	Artificial Neural Network
ANOVA	Analysis of Variance
BH	Static bed height
CFB	Circulating fluidized bed
GH	Gap height
ICFB	Internally circulating fluidized bed
ID	Internal Diameter
MLP	Multi-layer Perception model

an ICFB and observed an increment in the solid circulation rate with gas velocity. Song et al. [13] studied the effect of operating conditions, draft tube height, and distributor arrangement on the solid circulation rate and the gas bypassing between the draft tube and annular section. It was noted that higher draft tube height reduced the gas bypassing from the draft tube. Further, a correlation for the solid circulation rate was developed with the pressure drop across the gap opening and the opening ratio. Kim et al. [14] studied the influence of particle size and superficial velocities on the draft tube and annular section. It was found that the solid circulation rate rises with draft tube velocity due to the density difference between the draft tube and the annular section. In addition, a correlation based on Bernoulli's equation similar to Song et al. [13] was developed to predict the solid circulation rate, and the predicted value was within the 20% error range. Song et al. [15] measured the solids holdup and internal circulation rate in the upper surface of the ICFB by varying the air velocity, static bed height, and partition wall height using differential pressure transmitters and optical fiber probes. It was noted that the particle internal circulation rate increases with the static bed height and decreases with the partition wall height.

Jiang et al. [16] measured the particle circulation rate using the particle tracing method in a clapboard-type ICFB. The particle circulation rate was observed to increase initially and then decrease with a rise in the superficial velocity in a high-velocity zone. Li et al. [17] designed a novel high-temperature solar reactor with a clapboard-type internal circulating configuration. This work studied the effect of the bed mass and gas flow rate on thermal performance. They analyzed that increasing the superficial velocity enhances the particle circulation between the high and low-velocity regions. The pressure wave propagation in the vertical and horizontal direction using a self-designed clapboard-type Internal circulating fluidized bed was studied by Wei et al. [18]. It was observed that the superficial velocity influenced the pressure wave propagation in the vertical direction and had less influence on

the horizontal direction wave propagation. Chen et al. [19] focused on the effect of gas velocity in the draft tube and annular section, static bed height, and particle size on the solid's circulation rate. A dynamic model for internal particle circulation rate predicted the experimental data in the 20% error range.

In recent years, Machine learning has been used as an alternative to several experimental techniques to analyze large amounts of complex data within a limited time [20]. The advantage is understanding the relationship between process variables and measured values without conducting actual experiments. Artificial Neural Network (ANN) is one of the established techniques used for machine learning. Zhong et al. [21] predicted the solids holdup in a 10 m height circulating fluidized bed riser using ANN. The gas velocity, solids flux, and riser height were selected as the input parameters. It was observed that the proposed method gave better predictions under different test conditions. Chew et al. [20] applied the machine learning technique to identify the influence of process variables and the capability of the model to predict the fluidization data. The solids circulation rate was identified as the dominant factor influencing the solid concentration compared to the radial position and the solid segregation. A recent study by Mukesh et al. [22] predicted the circulating fluidized bed riser solid axial profile using ANN. The CFD-predicted data was initially used to train the data set used for the study. The input variables from the experimental data were the superficial velocity, solid circulation rate, and the riser height for the development of the ANN model. From the literature, it is found that the ANN studies focused on the predictions of solid holdup behaviors only in a circulating fluidized bed riser. ANN model usage for predicting solid circulation rate in the ICFB is absent.

1.1. Scope of the work

Very few theoretical studies in the literature focused on the solid circulation rate prediction in an Internal Circulating Fluidized Bed

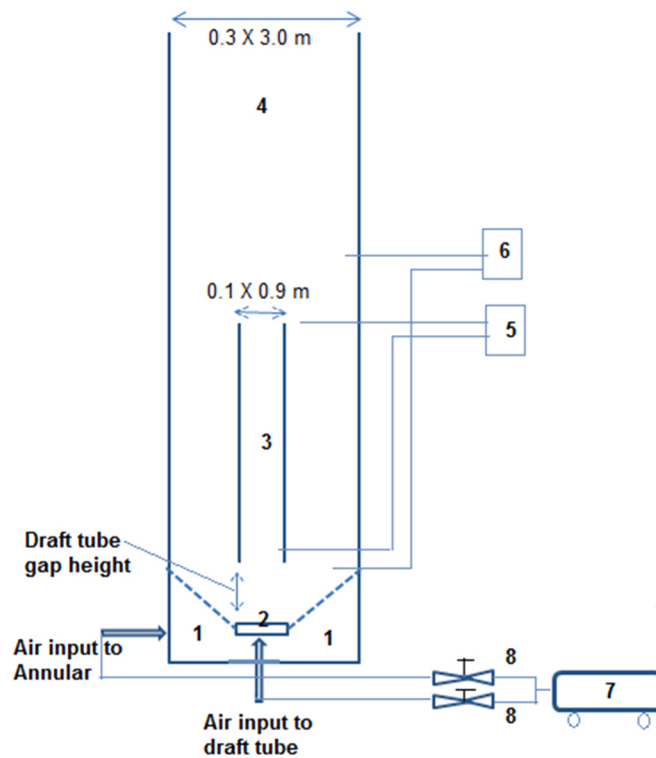


Fig. 1. Schematic diagram of ICFB with (1) annular air box (2) draft tube distributor (3) draft tube (4) ICFB (5) draft tube pressure measuring ports (6) annular bed pressure measuring ports (7) compressor (8) Air control value [23].

(ICFB) [15,16,19]. Those studies considered only pressure drop as the major contributor to the change in solid circulation rate and neglected other design and operational parameters. In general, it is influenced by several factors, including fluidized bed geometries, operating conditions, and properties of the bed material. Thus this study developed an empirical correlation based on the experimental results of Gujjula et al. [23] and expresses the solid circulation rate as a function of the above factors to identify the influence of the variables on the circulation rate. For this purpose, a dimensionless approach using Buckingham's π theorem and nonlinear regression models is adopted. Additionally, the Analysis of Variance (ANOVA) technique is used to check the significance level of the variables affecting the solid circulation rate. However, the empirical model predicting capability is limited. Also, it is not easy to develop an effective model if a nonlinear relationship exists between input and output parameters [24].

Alternatively, neural networks can analyze large amounts of data with complex features and extract various patterns in a relatively short period. As a result, they are helpful for a wide range of industrial applications, including predicting certain behaviors, detecting errors in data, etc. [25]. It also has excellent potential to reduce the efforts in experiments and simulation [26]. Thus in this work, the ANN model is adopted, and the Pearson correlation coefficient and Random Forest out-of-bag permuted predictor calculations help to analyze the

Table 1
Experimental operating conditions [23].

Parameters	Values
Gas superficial velocity (m/s)	0–2.8
Static bed height (m)	0.40, 0.50, 0.60
Draft tube height (m)	0.6
Draft tube gap height (m)	0.075, 0.105, 0.145
Particle mean diameter (μm)	470 800
Minimum fluidization velocity (m/s)	0.158 0.385
Density (kg/m^3)	2500 2550
Voidage	0.46 0.44

importance of variables in the order of their influence on the solid's circulation rate. Finally, a comparative analysis of the predicted solid circulation rate by empirical correlation and ANN with experimental measurements is performed. In addition, the developed empirical and ANN model solid circulation rate predictions are compared against literature-based experimental data, an independent study [27].

2. Methodology

2.1. Experimental methods

Fig. 1 represents the schematic diagram of the ICFB with the central draft tube used for experimental studies [23]. The experimental setup consists of a draft tube distributor, central draft tube, circulating fluidized bed main column, pressure measuring ports, compressor, and an air control valve. The experiments were conducted in a column made of Plexiglas to observe the circulation of particles inside the bed. It consists of the main column (0.3 m ID x 3.0 m high) and a central draft tube (0.1 m ID and 0.6 m height). Also, a conical air distributor with an inclined angle of 60° to horizontal with 72 perforations (2.45 mm ID) made of acrylic was used to supply air to the annulus section. A distributor plate with seven bubble caps is used for the air supply to the draft tube with a 0.1 m inner diameter. Each of these bubble caps has four holes of 2.4 mm inner diameter and is conical to prevent the accumulation of particles on the top of the cap.

The particles were fluidized using the compressed air from a 30 HP compressor. Initially, the air was supplied to the central draft tube. Once the fluidization started in the draft tube, the gas at a flow rate of 150 lpm was provided at the annular air distributor. The airflow rate was measured using the turbine flow meter ($6.4\text{--}48 \text{ m}^3/\text{h}$) and controlled by a gate valve. A pressure regulator for the storage tank of 1000 L capacity was used to avoid pressure fluctuations during the flow. Pressure drop within the draft tube and the annular section was measured using a U-tube manometer with water as the medium. In the study of Gujjula et al. [23], they attempted to capture low-frequency and high-fluctuating pressure signals that are significant and measurable by U-tube manometers. Further, all the experimental runs were made three times, and averaged pressure head data were tabulated to account for fluctuations. Sand particles with a mean diameter of 470 and 800 μm were used for this study. The water displacement method was selected to measure the particle density and voidage of the sand particles. The experimental operating conditions and particle data are provided in Table 1.



Fig. 2. Annulus moving bed velocity measurement (a) schematic diagram (b) experimental measurement of annular velocity [23].

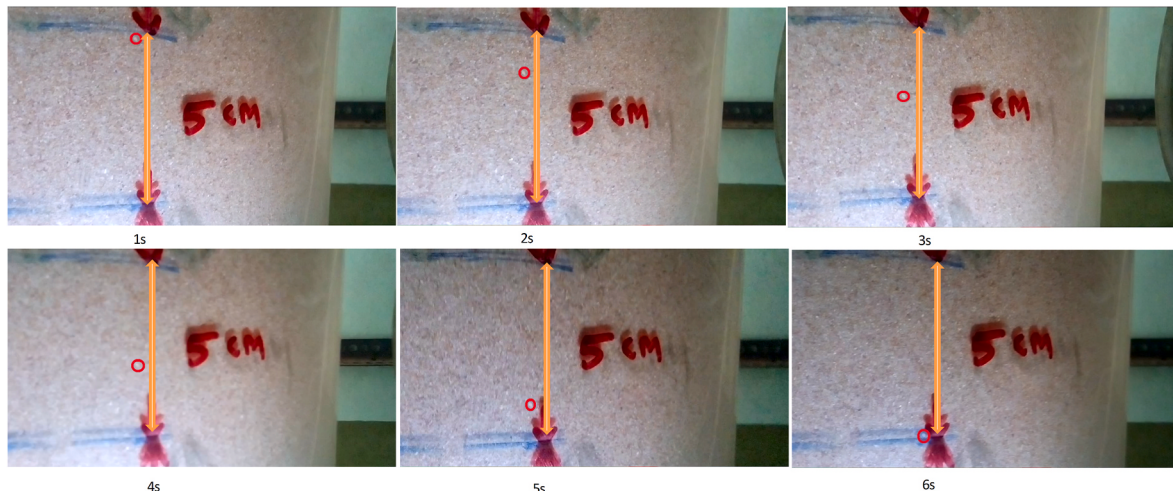


Fig. 3. Annular downward particle tracking at a fixed distance of 5 cm at different periods: 1 s, 2 s, 3 s, 4 s, 5 s, and 6 s [23].

2.2. Measurement of solid circulation rate

The solids circulation rate inside the bed was determined by measuring the downward-moving bed particle velocity [23]. As shown in Fig. 2, the downward-moving bed particle velocity was obtained by calculating the average time taken by the particles present at the annulus wall interface to move a distance of 5 cm in the downward direction. Once the particles fall from the riser/draft tube to the annular region, all particles move downward towards the bottom of the ICFB and enter into the draft tube through the gap opening at the bottom. In the annular zone, the entire bed behaves like a dense moving packed bed. In Fig. 3, a single tracer particle was tracked using a high-speed camera (Photron's FASTCAM SA1.1 model 675 K color having a 5000 fps at one

megapixels resolution) and measured the time required to travel a fixed distance of 5 cm. This procedure was repeated in three locations of the periphery of the ICFB column, and each experiment was performed three times, and the average time was noted down [13,14,28]. From this average time, the particle's downward velocity (U_{pAn}) was calculated and used in Eq. (1) to find the solids circulation rate (G_s). Downward particle velocity measurement in the annular section is shown in Fig. 3 for different periods.

After measuring the downward particle velocity, the solids circulation rate was calculated by Eq. (1),

$$G_s = U_{pAn}(1 - \varepsilon_s)\rho_s \quad (1)$$

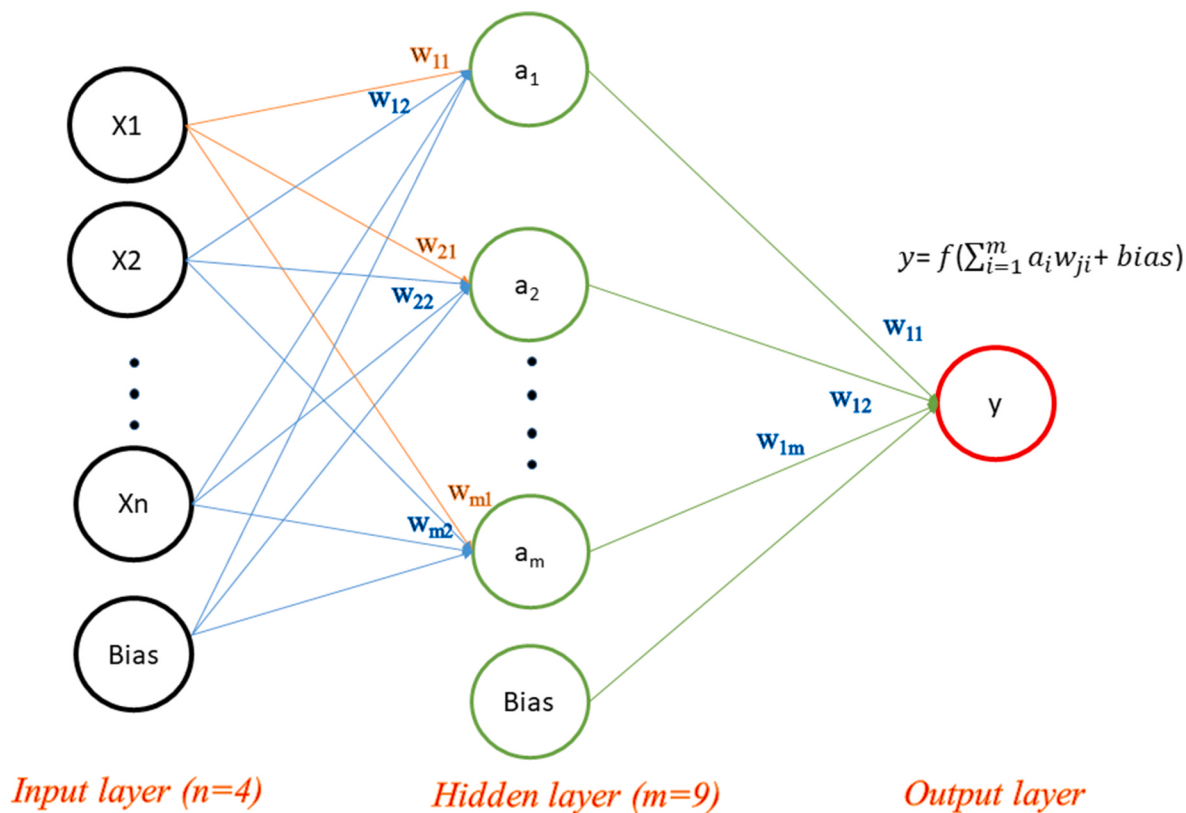


Fig. 4. Schematic diagram of ANN structure.

Table 2
Range of Input and Output variables used in the ANN model.

Input variables	Range
Average particle size, d_p (μm)	470, 800
Static bed height, BH (m)	0.4–0.6
Gap height, GH (m)	0.075–0.145
Superficial velocity, u_0 (m/s)	2.05–2.40
Output variable	Range
Solid circulation rate, G_s ($\text{kg}/\text{m}^2\text{s}$)	2.11–27.6

Table 3
Details of methods used in the ANN model.

No:	Parameters	Specifications
1	Network type	Feedforward Back Propagation
2	Training function	TRAINLM
3	Adaptive learning function	LEARNDNM
4	Performance function	MSE
5	Transfer function	TANSIG
6	Data division	Random (70:15:15)
7	No. of epoch	1000 iterations

Where,

ρ_s - density of solids (kg/m^3)

ε_s -solid volume fraction (-)

U_{pAn} -downward particle velocity in the annulus (m/s)

The annular bed region is not in a fluidized state but was assumed to

Table 4
Parameters with units and dimensions.

Parameter	Unit	Dimension
Solid circulation rate (G_s)	$\text{kg}/\text{m}^2\text{s}$	$\text{ML}^{-2}\text{T}^{-1}$
Superficial gas velocity (u_0)	m/s	LT^{-1}
Gas velocity in annular section (u_a)	m/s	LT^{-1}
Particle velocity in the riser (u_{pr})	m/s	LT^{-1}
Minimum fluidization velocity (u_{mf})	m/s	LT^{-1}
Gap area for the gas to flow (A_{Gap})	m^2	L^2
Static bed height (BH)	m	L
Solid particle diameter (d_p)	m	L
Solid particle density (ρ_s)	kg/m^3	ML^{-3}
Fluid density (ρ_f)	kg/m^3	ML^{-3}
Draft tube area (A_d)	m^2	L^2
Annulus area (A_a)	m^2	L^2
Draft tube height (H)	m	L
Fluid viscosity (μ)	$\text{kg}/\text{m s}$	$\text{ML}^{-1}\text{T}^{-1}$
Acceleration due to gravity (g)	m/s^2	LT^{-2}

behave in a descending nature. Therefore, this study took a volume fraction at the packed bed condition.

As the focus of the work is to develop an empirical correlation and ANN model by utilizing the experimental data of Gujjula et al. [23], experimentally measured draft tube pressure drop, annulus pressure drop, and solid circulation rate at different operating (gas velocities, particle diameters, static bed height) and design (draft tube height, gap height) conditions are not included in this paper for brevity. The complete data is available in the published work of Gujjula et al. [23].

Table 5

Fitted constants from the experimental data.

Parameter	i	j	k	m	o	s	p	q	w	Constant
Value	0.412	0.055	0.169	2.271	0.815	0.003	1.168	0.0734	1.255	5.54

2.3. Artificial Neural Network design

To develop the ANN model, **four variables, i.e., particle diameter, gap height, static bed height, and superficial velocity, are selected as the input parameters, and the solid circulation rate as the desired output.** The design, training, and validation of the data are performed using the neural network toolbox available in MATLAB R2020. Fig. 4 depicts a schematic diagram of the ANN structure. The range of the variables used in model development is provided in Table 2.

It is noted from the literature that the **multi-layer perceptron (MLP) Feedforward ANN is widely used in fluidization, where the signals are transmitted only in one direction, i.e., from the input layer through the hidden layer and finally to the output [29–31].** Further, the Back-propagation algorithm computed the error between the desired and actual output obtained. It adjusts the coefficients of weights and biases until the Mean Square Error (MSE) reaches a predetermined value. Therefore from the different neural network types, the widely used MLP [29–32] is selected in this study.

This network type typically consists of input, hidden, and output layers, and neurons are used to connect these layers. Initially, the input data of the independent variable is provided to the first layer. After completing the mathematical process on the received input, the hidden layer transfer the data to the output. The mathematical equation used to calculate the output from ANN is given in Eq. (2).

$$y = f \left(\sum_{i=1}^m a_i w_{ji} + bias \right) \quad (2)$$

where,

a_i - Input information to neuron

w_{ji} - Weight coefficient

y - output

f - transfer function

The present study employs the Feedforward Back Propagation learning rule. The network is first trained with the experimental data. Further, the output variables and the error obtained are measured. The same selected network is tested with different experimental values and checked for the reproducibility of the results.

The hidden neurons are represented using the format of 4×1 , where 4 is the number of input neurons, x is the number of neurons in the hidden layer, and 1 is the number of output neurons. The number of hidden neurons in a network and the number of neurons in each hidden layer are important factors in determining the overall network performance. Of the 66 data samples obtained from the experiments, **70% are used for training, 15% for validation, and 15% for testing.** Table 3 represents the parameters and specifications used for the ANN model.

3. Results and discussion

Initially, a dimensionless approach is used to establish the relationships between the solid circulation rate and the operating and design variables. This technique has the advantage of producing dimensionally consistent results for scale-up. Furthermore, a large quantum of experimentation is generally required to efficiently establish a relationship between the variable groups for a given range.

3.1. Dimensional analysis

The most commonly changed variables for ICFBs are **superficial velocity, annular velocity, particle diameter, bed height, the density of solid, the density of the fluid, gap height, area of gap height, area of the annular section, area of the draft tube, draft tube height, and viscosity.** The study conducted by Yang and Kearn [33] proved that the influence of the distributor angle on the solid circulation rate is negligible. The dimensionless groups like the Reynolds number and Richardson number and the variables like velocity, height, and area ratios are defined to develop various fluidized bed model structures to predict the solid circulation rate. Here, the Reynolds Number (Re) is given by Eq. (3), and the Richardson number (R_i) is given by Eq. (4).

$$Re_p = \frac{d_p u_{mf} \rho_f}{\mu} \quad (3)$$

$$R_i = \left(\frac{g \sqrt{A_d}}{u_{mf}^2} \right) \quad (4)$$

Buckingham's π theorem states that if n is the number of physical variables in an equation and k is the rank of the dimensional matrix, then p is the dimensionless parameters constructed from the original variables and is given by Eq. (5),

$$p = n - k \quad (5)$$

This is a scheme used for non-dimensionalization. This method helps to compute any sets of dimensionless parameters from the given variables, even though the form of the equation is still unknown. However, the choice of dimensionless parameters is not unique. **This theorem generates a set of dimensionless parameters, but the major drawback is that it fails to choose the most physically meaningful parameters.**

The three main primary dimensions of mass (M), length (L), and time (T) of the operating and design parameters are used for the development of the dimensionless variables. Table 4 provides the details of different parameters and their units and dimensions.

By using the Buckingham π theorem; Dimensionless variables are

$$\pi_1 = \frac{G_s}{(1 - \varepsilon_{mf}) u_{mf} \rho_s}, \pi_2 = \frac{U_{pr}}{U_0}, \pi_3 = \frac{U_a}{\sqrt{\frac{\Delta p}{(\rho_s - \rho_f)} A_d}}, \pi_4 = \frac{B_H}{\sqrt{A_d}}, \pi_5 = \frac{d_p}{\sqrt{A_d}},$$

$$\pi_6 = \frac{\mu}{u_{mf} \rho_s d_p}, \pi_7 = \frac{A_a}{A_d}, \pi_8 = \frac{H}{\sqrt{A_d}}, \pi_9 = \frac{g}{u_{mf}^2 \sqrt{A_d}}, \pi_{10} = \frac{A_{gap}}{A_d}$$

The term U_{pr} is calculated based on the equation provided below.

$$U_{pAn}(1 - \varepsilon_{An}) \rho_p A_{An} = U_{pr}(1 - \varepsilon_r) \rho_p A_r$$

Here, U_{pAn} represents particle velocity in the annulus, ε_{An} , ε_r represents bed voidage in the annulus and riser, and A_{An} and A_r represent the area of the annulus and riser.

The π terms can be represented as

$$f(\pi_1, \pi_2, \pi_3, \pi_4, \pi_5, \pi_6, \pi_7, \pi_8, \pi_9, \pi_{10}) = 0 \quad (6)$$

Based on the dimensional analysis, the above equation can be rewritten as

$$\pi_1 = f_1(\pi_2, \pi_3, \pi_4, \pi_5, \pi_6, \pi_7, \pi_8, \pi_9, \pi_{10}) \quad (7)$$

The effect of the operating and design parameters on the solid circulation rate in an ICFB can be expressed using the mathematical form.

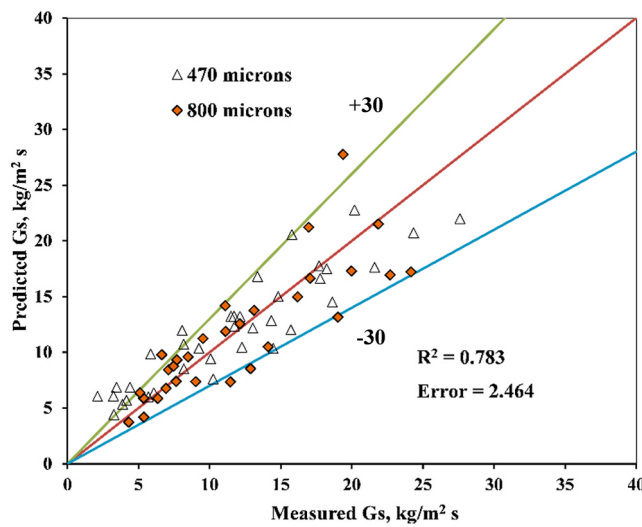


Fig. 5. Predicted G_s by the model compared with experimental data.

The main dependent Π_1 group is expressed in the undetermined function comprising the other 9 π terms. For the generalized relationship, the equation is written as a nonlinear relationship, and the p terms with coefficients i, j, k, m, o, s, p, q, w are shown in Eq. (8):

$$\frac{G_s}{\rho_s(1-\varepsilon_{mf})u_{mf}} \alpha \left(\frac{u_{pr}}{u_0} \right)^i \left(\frac{u_a}{\sqrt{\frac{\Delta p}{(\rho_s - \rho_f)}}} \right)^j \left(\frac{A_{gap}}{A_d} \right)^k \left(\frac{d_p}{\sqrt{A_d}} \right)^m \left(\frac{BH}{\sqrt{A_d}} \right)^o \left(\frac{\mu}{\rho_f d_p u_{mf}} \right)^s \left(\frac{A_a}{A_d} \right)^p \left(\frac{H}{\sqrt{A_d}} \right)^q \left(\frac{g\sqrt{A_d}}{u_{mf}^2} \right)^w \quad (8)$$

The above Eq. (8) can be rewritten as

$$\frac{G_s}{\rho_s(1-\varepsilon_{mf})u_{mf}} = Con^* \left(\frac{u_{pr}}{u_0} \right)^i \left(\frac{u_a}{\sqrt{\frac{\Delta p}{(\rho_s - \rho_f)}}} \right)^j \left(\frac{A_{gap}}{A_d} \right)^k \left(\frac{d_p}{\sqrt{A_d}} \right)^m \left(\frac{BH}{\sqrt{A_d}} \right)^o \left(\frac{1}{Re_p} \right)^s \left(\frac{A_a}{A_d} \right)^p \left(\frac{H}{\sqrt{A_d}} \right)^q \left(\frac{g\sqrt{A_d}}{u_{mf}^2} \right)^w \quad (9)$$

3.2. Model equations

The set of dimensionless variables included in the solid circulation

Table 6

Fitted constants from the experimental data.

$$\frac{G_s}{\rho_s(1-\varepsilon_{mf})u_{mf}} = 0.006^* \left(\frac{u_{pr}}{u_0} \right)^{0.425} \left(\frac{A_{gap}}{A_d} \right)^{0.034} \left(\frac{d_p}{\sqrt{A_d}} \right)^{0.159} \left(\frac{BH}{\sqrt{A_d}} \right)^{0.643} \left(\frac{A_a}{\sqrt{A_d}} \right)^{0.378} \left(\frac{g\sqrt{A_d}}{u_0^2} \right)^{0.542} \quad (11)$$

Parameter	i	j	k	m	o	s	p	q	w	Constant
Significance level (1-P)	0.999	0.745	0.974	0.955	0.994	0.073	0.827	0.996	0.994	-
Refitted constants after P-test	0.425	0	0.034	0.159	0.643	0	0.378	0	0.542	0.006

rate model is.

3.3. Dimensionless variables

Reduced particle diameter, $\left(\frac{d_p}{\sqrt{A_d}} \right)$	Reduced bed height, $\left(\frac{BH}{\sqrt{A_d}} \right)$
Reduced draft tube height, $\left(\frac{H}{\sqrt{A_d}} \right)$	Reduced gap area, $\left(\frac{A_{gap}}{A_d} \right)$
Reduced annular velocity, $\left(\frac{u_a}{\sqrt{\frac{\Delta p}{(\rho_s - \rho_f)}}} \right)$	Reduced annulus area, $\left(\frac{A_a}{A_d} \right)$
Reynolds number, $\left(\frac{d_p u_{mf} \rho_f}{\mu} \right)$	Richardson number, $\left(\frac{g\sqrt{A_d}}{u_{mf}^2} \right)$

The square root of the draft tube area $\sqrt{A_d}$ is chosen as the characteristic dimension of length.

The relationships between the dependent and independent variables are investigated using EXCEL SOLVER (Multiple linear fitting routines). It is corrected by minimizing the sum of the squares error between measured values to the model predicted values. This is generally known as regression analysis. The fitting routine estimates the parameter values in the equation tested. By considering all the practical fluidized model's other researchers developed and the latest test results, the following constants are fitted and displayed in Table 5. The final model equation is the best according to the fitting statistics. The solids circulation rate predicted by the fitted model for 470, 800 μm particles and corre-

sponding experimental data is depicted in Fig. 5. It can be observed that the model predictions are within the error limit of 30% of experimental data.

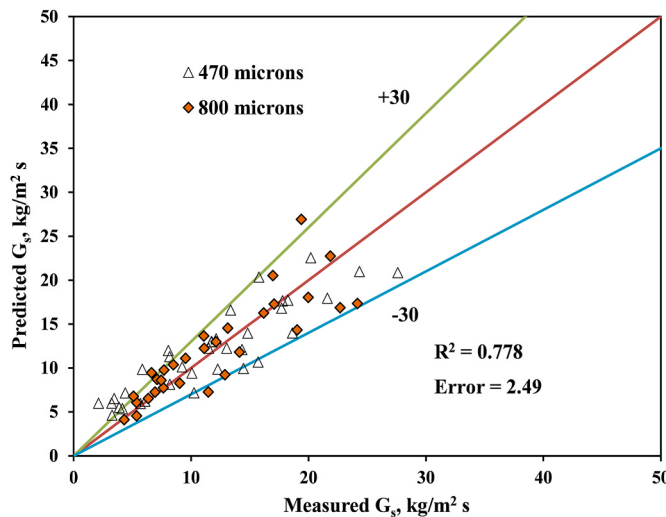


Fig. 6. Predicted G_s by the model after the significance test compared with experimental data.

3.4. ANN model predictions

3.4.1. Neural network design

The selection of the appropriate number of neurons and the hidden layer is a key factor in designing the MLP neural network. Four input variables (particle diameter, gap height, static bed height, and superficial velocity) are selected in this case, and the solid circulation rate is the desired output variable. This study obtains the best result with a single hidden layer consisting of nine neurons. A comparison between the experimental results and the ANN model predicted data is given in the regression plot as shown in Fig. 7. It is observed that the predicted ANN model results in an overall R^2 -value of 0.955 (Fig. 7), with convergence occurring at the 18th epoch. After obtaining the best ANN topology, the test data is introduced into the network to compare the experimental and ANN-predicted values of the solid's circulation rate.

The weight factor and biases used in the proposed ANN model are:

$$\frac{G_s}{\rho_s(1-\varepsilon_{mf})u_{mf}} = 5.54 * \left(\frac{u_{pr}}{u_0}\right)^{0.412} \left(\frac{u_a}{\sqrt{\frac{\Delta p}{(\rho_s - \rho_f)}}}\right)^{0.055} \left(\frac{A_{gap}}{A_d}\right)^{0.169} \left(\frac{d_p}{\sqrt{A_d}}\right)^{2.271} \left(\frac{BH}{\sqrt{A_d}}\right)^{0.815} \left(\frac{1}{Re_p}\right)^{0.003} \left(\frac{A_a}{A_d}\right)^{1.168} \left(\frac{H}{\sqrt{A_d}}\right)^{0.0734} \left(\frac{g\sqrt{A_d}}{u_{mf}^2}\right)^{1.255} \quad (10)$$

The Analysis of Variance (ANOVA) technique is used to calculate F-number and their corresponding probabilities (P-values), thereby identifying the insignificant variables in the empirical model (Eq. (10)). Suppose the significance levels ($1-P$) of at least one fitted constants are greater than 0.95; those terms are considered significant in the model. If the significance levels are less than 0.95, then the terms are considered insignificant and fitted constants are assumed to be zero. The significance levels and refitted constants of each parameter after the significance test are displayed in Table 6. The final model is shown in Eq. (11). The corresponding G_s model is assessed in terms of goodness of fit, fitting statistics, and improvement over existing parameters. The solids circulation rate predicted by the modified model after the significant test for 470, 800 μm particles and corresponding experimental data is presented in Fig. 6. It can be observed that the modified model predictions are also within the error limit of 30% of experimental data.

$$w1 = \begin{bmatrix} 1.4233 & 0.9890 & 0.8622 & -1.5589 \\ -0.8116 & 1.3621 & -2.8383 & 1.4004 \\ -2.4495 & 1.1111 & -0.0612 & -0.3859 \\ -2.3296 & -0.0414 & -0.517 & 2.1951 \\ -0.3936 & 1.716 & -0.6099 & -2.5604 \\ -0.6449 & -1.3522 & 2.1323 & 0.0888 \\ -0.7671 & 3.1791 & -1.6185 & -1.1155 \\ 0.9599 & -1.4243 & 0.8269 & -0.1772 \\ 0.5903 & 0.2990 & 0.2937 & 2.7054 \end{bmatrix}$$

$$b1 = \begin{bmatrix} -2.0617 \\ 1.2976 \\ 1.5612 \\ 0.3568 \\ 0.7295 \\ -0.0065 \\ -1.3894 \\ 1.6743 \\ -2.8915 \end{bmatrix}$$

$$w2 = [-0.6473 \quad 0.2405 \quad -0.3362 \quad 2.5343 \quad -0.2599 \quad 0.6413 \quad -1.2785 \quad -2.0027 \quad 2.5588]$$

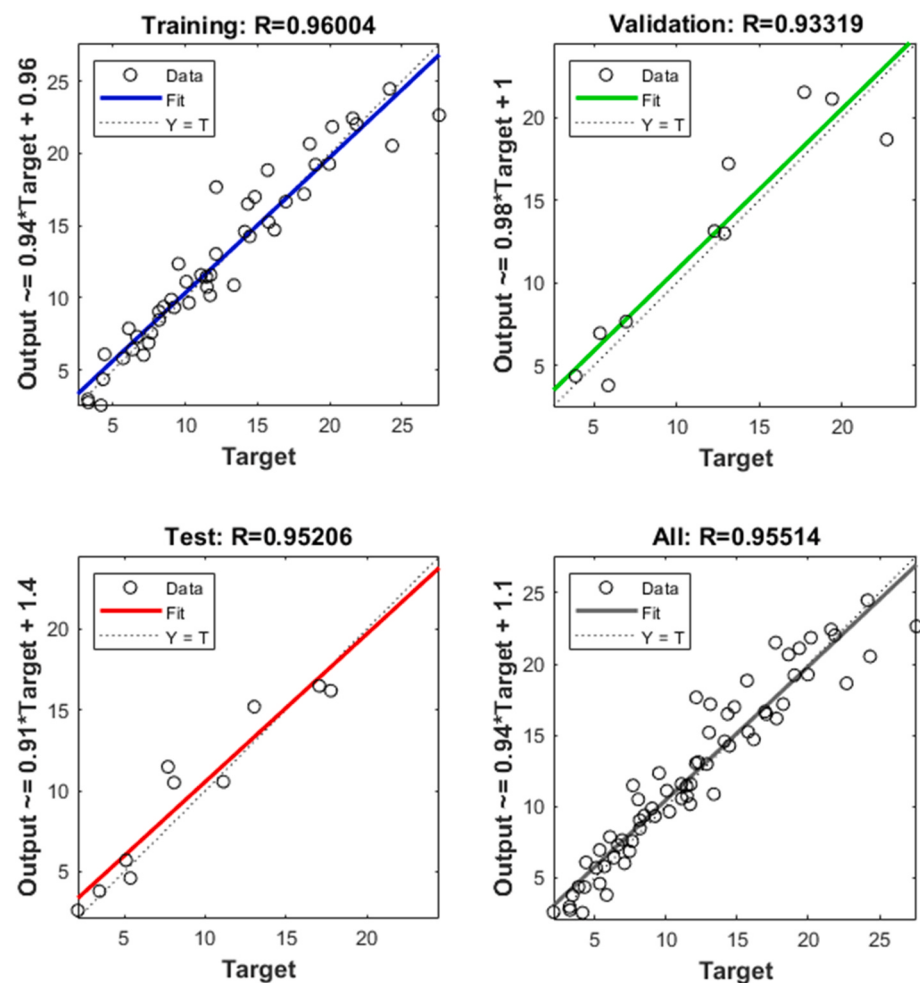


Fig. 7. ANN regression plot.

Table 7

Values of Pearson correlation coefficient between the variables and solids circulation rate.

Variables	Pearson correlation coefficient
Particle diameter	0.021
Superficial gas velocity	0.549
Gap height	0.124
Static bed height	0.341

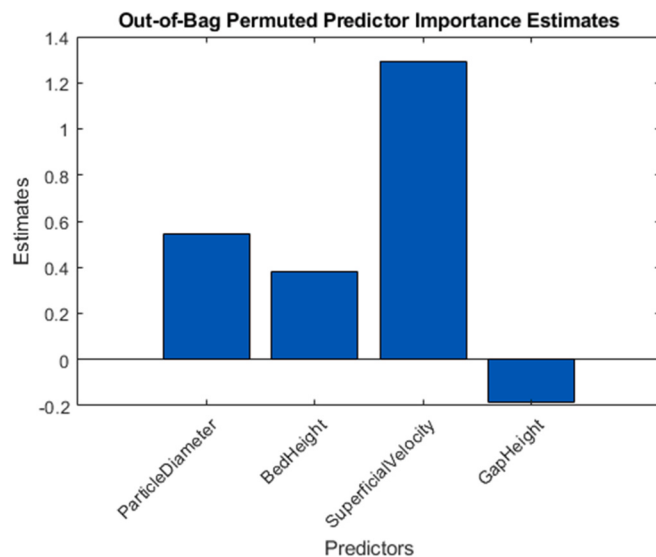


Fig. 8. Random Forest out-of-bag permuted predictor importance estimates for solids circulation rate.

$$b2 = [-0.6076]$$

3.4.2. Correlation analysis

The relationship between the independent and the dependent variables is measured using the Pearson correlation coefficient values [34]. This coefficient determines the magnitude of the association and the direction of the relationship between the variables. The correlation coefficient takes the values between -1 and $+1$. A value of $+1$ denotes a strong positive relation, while -1 denotes an inverse relation, and zero indicates no relationship between the variables. In this study, the Pearson correlation coefficient is used to determine the relationship between the independent variables i.e. particle diameter, gap height, static bed height, and superficial velocity to solids circulation rate. The Pearson correlation coefficient (r) value is provided in Table 7. It is noted that from the four independent variables, the superficial velocity shows a higher value and is closely related to the solid's circulation rate.

The random forest out-of-bag permuted predictor important estimates give the significance of the variables in predicting the output parameter [35]. Fig. 8 represents the out-of-bag permuted predictor importance estimates of solids circulation rate. In the order of the variable importance, the superficial velocity is the most dominant, followed by the particle diameter and the static bed height. This shows that the

superficial velocity is crucial in determining solid circulation rate, which is also true from the Pearson's correlation value obtained, as shown in Table 7. It is also observed from the figure that the gap height is the variable with the least significance.

3.4.3. Model evaluation

The developed MLP neural network and empirical correlation are further tested to predict the solid circulation rate (unused data) within the limits of operating and design conditions used for model developments. Fig. 9 compares the ANN model, and the empirical model predicted solid circulation rate against the experimental values for different static bed heights of $470\text{ }\mu\text{m}$ particles. It is clear from the figure that the ANN predicted values show close predictions with the experimental compared to the empirical model predictions. At a bed height of 0.4 m , an error of 28.7% is obtained with the empirical model and reduced to 9.49% using the ANN model. Further, for 0.5 m bed height, it is noted that an error of 5.78% is obtained by comparing the experimental and ANN predicted values (Fig. 9b). A similar behavior can be observed for the other gap heights and particle sizes (Fig. 9c and d).

In Fig. 10, the reliability of empirical and ANN model solid circulation rate predictions are tested against the literature-based experimental data of Chandel and Alappat [27]. It can be observed that the empirical model predictions deviate from the experimental values, although it shows an increasing trend. The empirical model deviation may be due to the experimental solid circulation data [27] generated at different operating conditions and design parameters. In general, the empirical correlations fit systematically only to modeled experiments, and the predictions are restricted to experiments under specific operational conditions. In ANN, this range of experimental conditions can be expanded by adding new sets of experimental data in training [36]. In this work, 50% of new experimental data is used for training the proposed ANN model without changing the weight factors and biases. With its generality and ability to interpolate different operating and design conditions, the ANN model gives better predictions for solid circulation rate than the empirical model.

4. Conclusions

This study developed an empirical correlation for the solid circulation rate in an ICFB using a non-dimensional approach and nonlinear regression analysis. ANOVA is utilized to identify the significant variables affecting the solid circulation rate. The modified empirical model with significant variables predicted the experimental data within $\pm 30\%$ error limits for both 470 and $800\text{ }\mu\text{m}$ particles. Further, the same experimental data is utilized to generate an ANN model with the MLP algorithm to predict the solid circulation rate. Out of the total data samples, 70% of data are used for training, 15% for validation, and 15% for testing. An overall R -value of 0.955 is obtained using the ANN model, and a good fit of the experimental data to the model predicted is observed in training and testing. A good comparison with an error of less than 7.8% is noted between the experimental and ANN-predicted values at different static bed heights for the gap height of 0.075 m and $470\text{ }\mu\text{m}$ particles. Pearson correlation coefficient and Random Forest out-of-bag permuted predictor calculations indicated that superficial gas velocity is the statistically significant parameter and dominant factor affecting solid circulation rate over particle size, gap height, and static bed height. In addition, the reliability of the developed empirical and ANN model on the prediction of solid circulation rate is compared against literature-

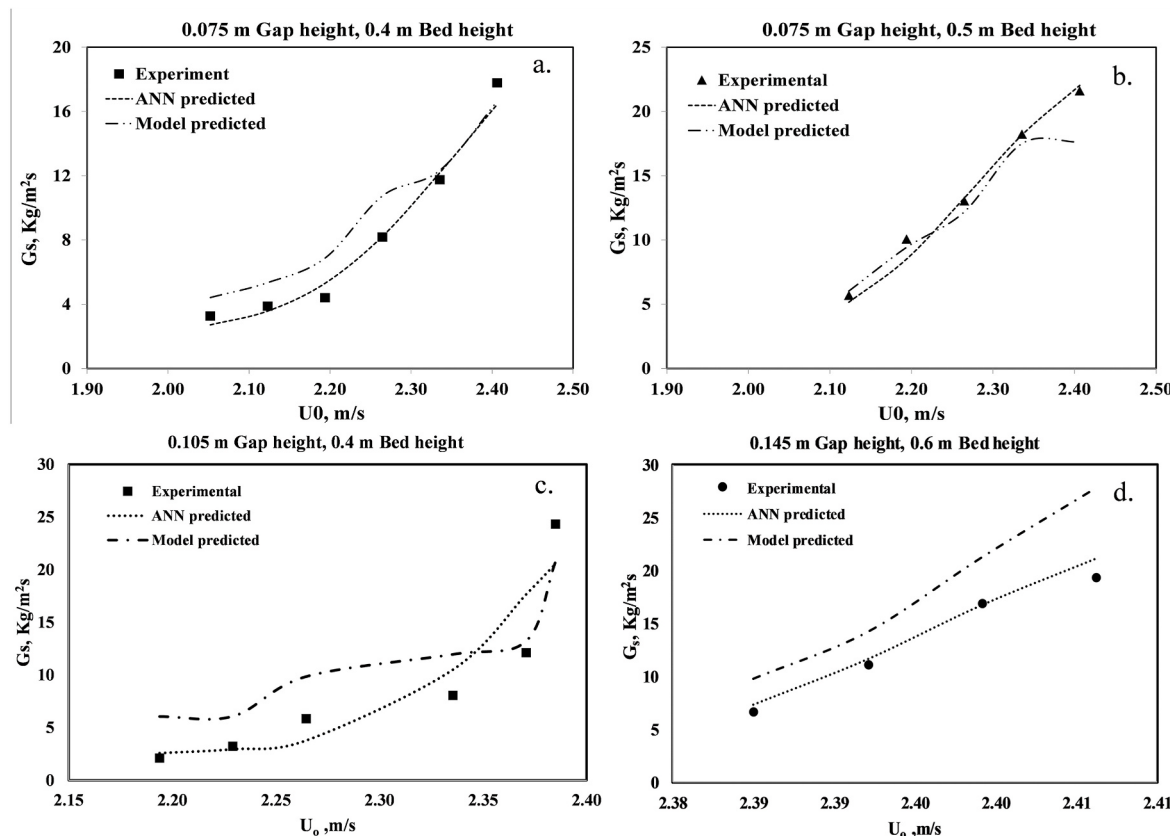


Fig. 9. Cross-validation of the empirical model and ANN predicted solid circulation rate against experimental data for 470 μm (a,b and c) and 800 μm (d) particles.

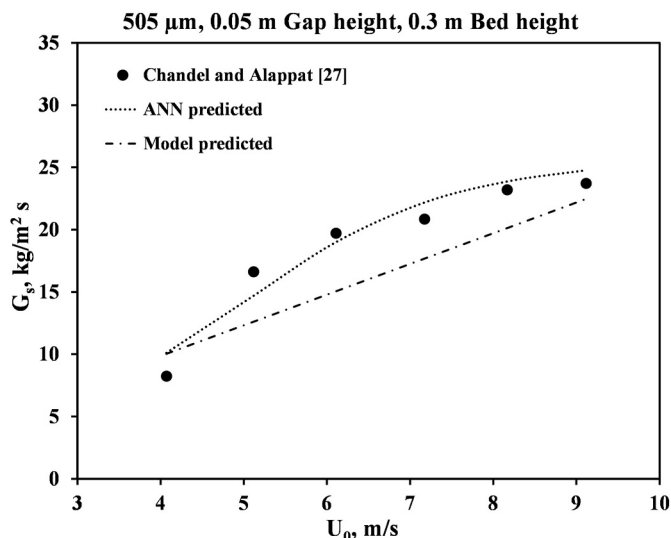


Fig. 10. Comparison of the developed empirical and ANN model predictions with the literature data of Chandel and Alappat for solid circulation data (G_s) [27].

based experimental data. The results show that the ANN model could provide better predictions with desirable accuracy than the empirical model.

Credit author Statement

Mona Mary Varghese: Methodology, Investigation, Data curation, Writing – original draft. Teja Reddy Vakamalla: Conceptualization, Resources, Supervision, Writing-Review, and editing. Ravi Gujjula: Data curation, Writing-Review. Narasimha Mangadoddy: Resources and editing

Declaration of competing interest

The authors declare that they have no known competing financial interests or personal relationships that could have appeared to influence the work reported in this paper.

Data availability

Data will be made available on request.

Acknowledgments

The authors would like to express their sincere thanks to NIT Calicut and IIT Hyderabad for funding and support. The authors also thanks DST-FIST, SR/FIST/ET-1/2020/646, Govt. Of India., for their financial support.

References

- [1] D. Kunii, O. Levenspiel, Chapter 2 - industrial applications of fluidized beds, in: D. Kunii, O. Levenspiel (Eds.), *Fluidization Engineering*, Butterworth-Heinemann, Boston, 1991, pp. 15–59.
- [2] Y. Feng, T. Swenser-Smith, P.J. Witt, C. Doblin, S. Lim, M.P.J.P.T. Schwarz, CFD modeling of gas-solid flow in an internally circulating fluidized bed, *Powder Technol.* 219 (2012) 78–85.

- [3] Y.J. Kim, J. Lee, S. Kim, Modeling of coal gasification in an internally circulating fluidized bed reactor with draft tube, *Fuel* 79 (2000) 69–77.
- [4] Y.T. Kim, B.H. Song, S.D. Kim, Entrainment of solids in an internally circulating fluidized bed with draft tube, *Chem. Eng. J.* 66 (2) (1997) 105–110.
- [5] B.H. Song, Y.T. Kim, S.D. Kim, Circulation of solids and gas bypassing in an internally circulating fluidized bed with a draft tube, *Chem. Eng. J.* 68 (2–3) (1997) 115–122.
- [6] S.D. Kim, Y.H. Kim, S.A. Roh, D.H. Lee, Solid circulation characteristics in an internally circulating fluidized bed with orifice-type draft tube, *Kor. J. Chem. Eng.* 19 (5) (2002) 911–916.
- [7] C. Chu, S. Hwang, Flue gas desulfurization in an internally circulating fluidized bed reactor, *Powder Technol.* 154 (2005) 14–23.
- [8] F. Miccio, G. Ruoppolo, S. Kalisz, L. Andersen, T. Morgan, D. Baxter, Combined gasification of coal and biomass in internal circulating fluidized bed, *Fuel Process. Technol.* 95 (2012) 45–54.
- [9] W. Tian, X. Wei, J. Li, H.Z. Sheng, Internal circulating fluidized bed incinerator system and design algorithm, *J. Environ. Sci.* 13 (2001) 185–188.
- [10] A. Reichhold, H. Hofbauer, Internally circulating fluidized bed for continuous adsorption and desorption, *Chem. Eng. Process* 34 (6) (1995) 521–527.
- [11] R. Gujjula, N. Mangadoddy, Hydrodynamic study of gas–solid internally circulating fluidized bed using multiphase CFD model, *Part. Sci. Technol.* 33 (6) (2015) 593–609.
- [12] Y.T. Choi, S.D. Kim, Bubble characteristics in an internally circulating fluidized bed, *J. Chem. Eng. Jpn.* 24 (2) (1991) 195–202.
- [13] B.H. Song, Y.T. Kim, S.D. Kim, Circulation of solids and gas bypassing in an internally circulating fluidized bed with a draft tube, *Chem. Eng. J.* 68 (2) (1997) 115–122.
- [14] S.D. Kim, Y.H. Kim, S.A. Roh, D.H. Lee, Solid circulation characteristics in an internally circulating fluidized bed with orifice-type draft tube, *Kor. J. Chem. Eng.* 19 (5) (2002) 911–916.
- [15] Y. Song, X. Lu, Q. Wang, J. Li, S. Sicong, X. Zheng, F. Yang, X. Fan, Experimental study on gas–solid flow characteristics in an internally circulating fluidized bed cold test apparatus, *Adv. Powder Technol.* 28 (2017).
- [16] G. Jiang, L. Wei, Z. Chen, L. Peng, N. He, C. Wu, Experimental investigation of particle circulation in an internally circulating clapboard-type fluidized bed, *Chem. Eng. Technol.* 43 (2) (2020) 253–262.
- [17] X. Li, L. Wei, C.W. Lim, J. Chen, P. Chu, W. Lipiński, N. Yan, Y. Dai, C.-H. Wang, Experimental and numerical study on thermal performance of an indirectly irradiated solar reactor with a clapboard-type internally circulating fluidized bed, *Appl. Energy* 305 (2022), 117976.
- [18] L. Wei, B. Zhang, C. Lu, Y. Lu, C.-H. Wang, Experimental investigation of pressure fluctuation propagation in two orthogonal directions using a clapboard-type internally circulating fluidized bed, *Adv. Powder Technol.* 31 (8) (2020) 3395–3407.
- [19] H. Chen, Y. Song, Y. Shi, X. Yang, Prediction of particle circulation rate in an internally circulating fluidized bed with a central draft tube, *Powder Technol.* 380 (2020).
- [20] J.W. Chew, R.A. Cocco, Application of machine learning methods to understand and predict circulating fluidized bed riser flow characteristics, *Chem. Eng. Sci.* 217 (2020), 115503.
- [21] H. Zhong, Z. Sun, J. Zhu, C. Zhang, Prediction of solid holdup in a gas–solid circulating fluidized bed riser by artificial neural networks, *Ind. Eng. Chem. Res.* 60 (2021).
- [22] M. Upadhyay, V.M. Nagulapati, H. Lim, Hybrid CFD-neural networks technique to predict circulating fluidized bed reactor riser hydrodynamics, *J. Clean. Prod.* 337 (2022), 130490.
- [23] R. Gujjula, N. Mangadoddy, Experimental investigation of hydrodynamics of gas–solid flow in an internally circulating fluidized bed, *Can. J. Chem. Eng.* 93 (8) (2015) 1380–1391.
- [24] O. Kisi, K.S. Parmar, Application of least square support vector machine and multivariate adaptive regression spline models in long term prediction of river water pollution, *J. Hydrol.* 534 (2016) 104–112.
- [25] M.G.M. Abdolrasol, S.M.S. Hussain, T.S. Ustun, M.R. Sarker, M.A. Hannan, R. Mohamed, J.A. Ali, S. Mekhilef, A. Milad, Artificial neural networks based optimization techniques, *Review* 10 (21) (2021) 2689.
- [26] M. Upadhyay, V.M. Nagulapati, H. Lim, Hybrid CFD-neural networks technique to predict circulating fluidized bed reactor riser hydrodynamics, *J. Clean. Prod.* 337 (2022), 130490.
- [27] M.K. Chandel, B.J. Alappat, A model for the solid circulation rate in a recirculating fluidized bed, *Chem. Eng. Commun.* 193 (12) (2006) 1514–1526.
- [28] H.-S. Ahn, W.-J. Lee, S.-D. KimDg, B.-H. Song, Solid circulation and gas bypassing in an internally circulating fluidized bed with an orifice-type draft tube, *Kor. J. Chem. Eng.* 16 (5) (1999) 618–623.
- [29] R. Mathew, M. Begum, A. Narayanan, Hydrodynamic studies on fluidized beds with internals: experimental and ANN approach, *Powder Technol.* 264 (2014) 423–429.
- [30] K. Korkerd, C. Soanuch, D. Gidaspow, P. Piomsomboon, B. Chalermsinsuwan, Artificial neural network model for predicting minimum fluidization velocity and maximum pressure drop of gas fluidized bed with different particle size distributions, *S. Afr. J. Chem. Eng.* 37 (2021) 61–73.
- [31] D. Serrano, I. Golpour, S. Sánchez-Delgado, Predicting the effect of bed materials in bubbling fluidized bed gasification using artificial neural networks (ANNs) modeling approach, *Fuel* 266 (2020), 117021.
- [32] A.B. Asghar, S. Farooq, M.S. Khurram, M.H. Jaffery, K. Ejsmont, Estimation of the solid circulation rate in circulating fluidized bed system using adaptive neuro-fuzzy algorithm, *Energies* 15 (1) (2022) 211.
- [33] W. Yang, Design of Recirculating Fluidized Beds for Commercial Applications, *AICChE Symp. Ser.*, 1978, pp. 218–228.
- [34] H. Liu, C. Chen, Y. Li, Z. Duan, Y. Li, Chapter 9 - characteristic and correlation analysis of metro loads, in: H. Liu, C. Chen, Y. Li, Z. Duan, Y. Li (Eds.), *Smart Metro Station Systems*, Elsevier2022, pp. 237–267.
- [35] S. Janitza, R. Hornung, On the overestimation of random forest's out-of-bag error, *PLoS One* 13 (2018), e0201904.
- [36] B. Silva, A. Fileti, O. Taranto, Drying of Brazilian pepper-tree fruits (*schinus terebinthifolius raddii*): development of classical models and artificial neural network approach, *Chem. Eng. Commun.* 202 (2015) 1089–1097.